URSI GASS 2021, Rome, Italy, 28 August - 4 September 2021

Miniaturized coils for noninvasive magnetic stimulation: a numerical comparison in terms of focality and penetration depth

Micol Colella*(1,2), Micaela Liberti (1), Daniel Z. Press (3), Francesca Apollonio (1) and Giorgio Bonmassar (2)

(1) Department of Information Engineering, Electronics and Telecommunications, Sapienza University of Rome, Rome, Italy;
(2) Athinoula A. Martinos Center for Biomedical Imaging, Massachusetts General Hospital, Boston, MA, USA;
(3) Department of Neurology, Beth Israel Deaconess Medical Center, Boston, MA, USA;

Abstract

Miniaturized multi-layered coils (*mCoils*) were designed to achieve focal noninvasive magnetic stimulation of neural tissue. Thus, overcoming the well-known spatial resolution limitations of standard transcranial magnetic stimulation (TMS). The first *mCoils* were manufactured using novel flex circuit technologies, and their efficacy and safety have been assessed experimentally in previous studies using peripheral nerve stimulation of healthy subjects. This paper examines the second upgraded generation of the *mCoils*, the *mTMS* coils, specifically designed to target the brain cortex by doubling the number of layers and increasing the coil diameter. Additionally, an iron core was introduced to increase the induced E-field intensity inside the brain. The *mTMS* coils were studied to estimate their focality and penetration depth inside a virtual head model. The results show that despite a larger coil diameter, the *mTMS* coils maintain the original *mCoil* focality.

1 Introduction

Transcranial magnetic stimulation (TMS) is a noninvasive brain stimulation technique that employs a high intensity pulsed magnetic field generated by a stimulating coil and traveling through the scalp [1]. According to Faraday's law, such a time-varying magnetic field induces an electric field inside the head, which can elicit a neuronal response [2]. TMS has been extensively adopted over the years for clinical purposes [3] and in the diagnostic field, and as a neuroinvestigative tool to understand network interactions. TMS revealed relations between brain activity and behavior, as in the cortical motor [4], [5], or language [6], [7] mapping. Furthermore, the diagnose of motor diseases, such as spinal cord injuries [8], can be performed through electromyographical recordings of the muscular stimuli induced by TMS (i.e., motor evoked potentials, MEPs). TMS has also been used in either inhibition or facilitation of language processes in healthy volunteers [7] or in patients affected by tumors [9], [10]. This procedure affords precise and individual language mapping, which is of paramount importance during brain tumor surgery to prevent or minimize neurological damage of language-eloquent areas [10].

Despite the great TMS potentials, a critical barrier is its limited focality, which strongly depends on the coil geometry and shape [11]. The coils commercially available and used in the clinics can have dimensions up to 20 cm, comparable with the size of the human head. Therefore, the induced E-field distribution over the brain leaks in regions surrounding the target area, containing inhibitory or facilitatory neuronal connections that may alter the expected stimulation outcome [11]. A high stimulation focality is also desirable in animals to study the cellular and molecular level changes that occur following prolonged TMS stimulations [12] and to understand the molecular mechanisms that underlie TMS's therapeutic effect on psychological and neurological disorders [13], [14]. Large coils expose the entire animal's body and reduce stimulation efficacy in target brain areas, which would capture a proportionally smaller fraction of the total magnetic field flux [15].

Several solutions have been proposed in the literature for reducing the dimensions of the stimulating coil [16]–[18]. However, the limitation in such smaller coils, with respect to larger ones, is that they require higher feeding currents with considerable power losses and overheating [19]. In order to avoid such caveats, alternative techniques must be employed. The basic principle is that the cut section of a wire is a circle, while the cut section of a flex trace is a rectangle. As we increase the number of turns, more wires/traces are stacked one on top of another. While rectangles can be stacked to produce virtually no gaps (e.g., brick wall), circles will always create gaps resulting in larger coils. Also, traces have the advantage of maintaining the same cross-sectional area of wires by reducing one size while increasing the other (i.e., thin but wide traces), thus allowing us to manufacture slimmer coils. The cross-sectional area of a conductor is a crucial design specification as it is inversely proportional to the coil's resistance and heating. Long, thin, and flexible traces are now part of the new generation of miniaturized coils, such as the miniaturized coil (*mCoil*) whose safety and efficacy have been demonstrated both numerically and experimentally by stimulating the radial nerve of healthy subjects [20], [21]. Furthermore, the new miniaturized coil (*mTMS* coil) was designed to be applied in the future to the human cortex [22]. We have studied both coils numerically to compare them in their focality and cortical penetration depth.

2 Materials and Methods

The first *mCoil* was built depositing four traces, wound in 123 turns around a copper pin with a 1 mm diameter, and trace thickness of just 25 µm and an overall resistance below 2 Ω. Since each layer was 1 mm high, with a distance of 0.5 mm between two adjacent layers, we fabricated a single 8 mm-tall circular solenoid with an outer diameter of 15 mm. A figure-8 stimulator was obtained by pairing two single solenoids, thus obtaining a structure with a maximum dimension of 30 mm. The geometry of *mCoil* has been improved by doubling the number of layers and winding them in 100 turns around an iron core to achieve higher E-field intensities. This new structure had an inner diameter of 9.5 mm and an outer diameter of 20.5 mm. The coil's height is 12.5 mm, and the length of the iron core is 45 mm, with 2 mm protruding from the coil towards the scalp.

For both the coils, the numerical model was built in the simulation software Sim4Life (v.5.0, Zurich MedTech, Zurich). Each copper trace was modeled as a planar loop coil and was placed in the middle of the corresponding trace. The space between two loops was chosen so to take into account the thickness of each trace and the space between adjacent traces. Finally, each coil was placed over the hand knob of the motor area M1 of the human head model MIDA [23], as shown in **Fig. 1**.

Electromagnetic (EM) simulations were conducted using Sim4Life Magneto Quasi-static solver with a 1.9 kHz sinusoidal excitation, chosen as a good approximation of the biphasic pulse. To quantify the electric field penetration depth and focality of the two miniaturized coils, we followed the definitions given in [24]. Here penetration depth is defined by the half-value depth, $d_{1/2}$, meaning the radial distance from the cortical surface to the deepest point where the electric field strength is half E_{max} on the cortex surface. The focality is defined as the half-value spread $S_{1/2} = V_{1/2}/d_{1/2}$, where $V_{1/2}$ is the half-value volume, meaning the volume of the brain region exposed to an electric field equal to or greater than $E_{max}/2$.

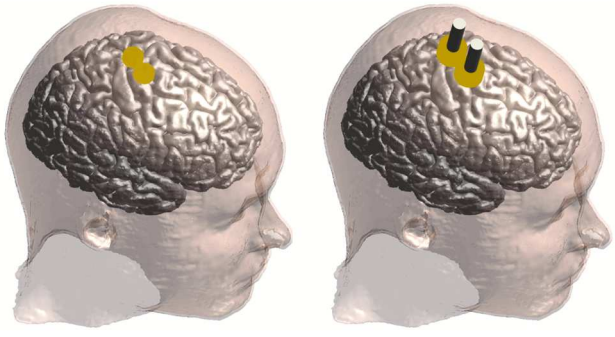

Figure 1. The numerical model of the *mCoil* (left) and *mTMS* coil (right). Both coils are placed over the hand knob of the primary motor cortex M1 of the human head model MIDA.

3 Results

All the results shown were normalized to the respective maximum E-field intensity. In **Fig. 2**, the electric field induced by the *mCoil* (top) and by the *mTMS* coil (bottom) on the grey matter's surface is reported. The two E-field distributions look similar, with the peak intensities focused over the hand knob and the two surrounding gyri's exposure. As expected, the area exposed to values above half of each respective maximum ($E_{max,mCoil}/2$ or $E_{max,mTMS}/2$) is slightly wider for the *mTMS* coil, as shown by the red contours in the inset of **Fig.2**. Similarly, the *mTMS* coil also induced an E-field that was able to reach deeper regions inside the brain with higher values with respect to the *mCoil*, as shown by the map reported in **Fig.3**. The depth reached by values above $E_{max}/2$ remained confined in a superficial area for both cases. From the target spot on the cortex, it is possible to define the half-value depth, $d_{1/2}$ as in [24], which corresponds to the distance from the deepest point in the brain that experienced an E-field intensity equal to half of the maximum value.

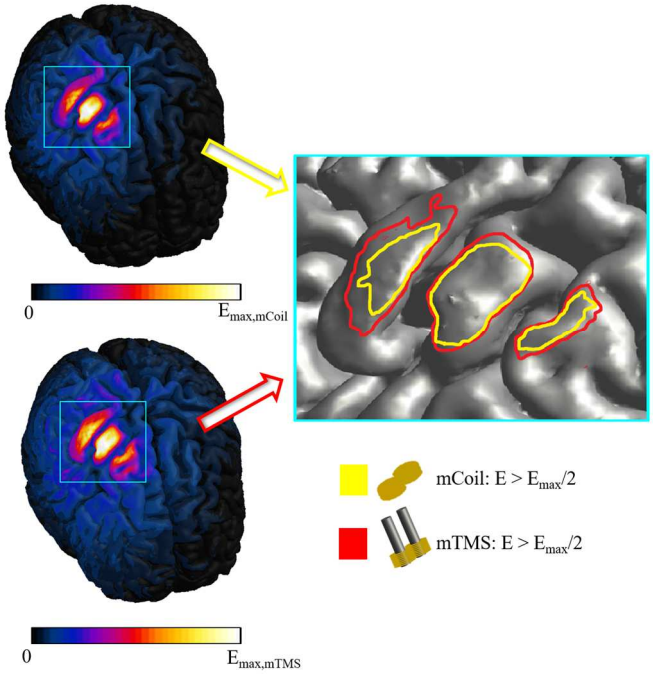

Figure 2. Distribution of the E-field induced on the surface of the cortex by the *mCoil* (top) and by the *mTMS* coil (bottom). Cyan inset shows isocurves delimiting the area of cortex exposed to intensities above $E_{max}/2$ for the two coils.

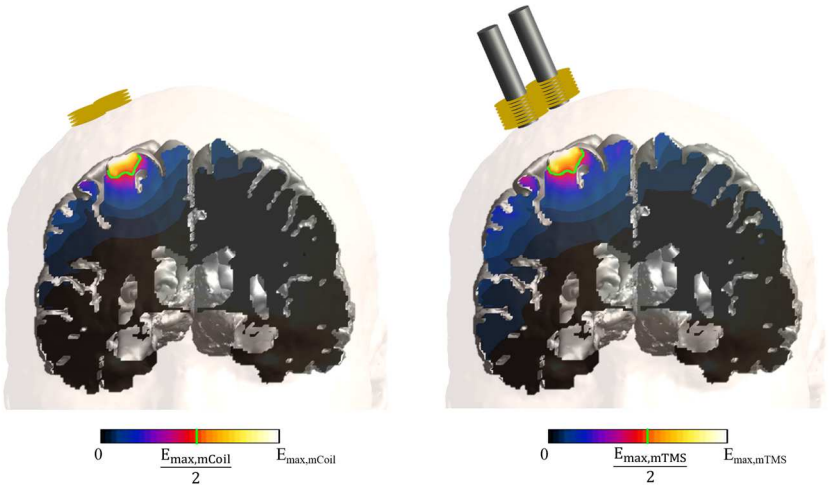

Figure 3. E-field map inside the brain over the coronal plane at the peak point. Left: *mCoil*; Right: *mTMS* coil. E-field intensities of $E_{max}/2$ are highlighted in green.

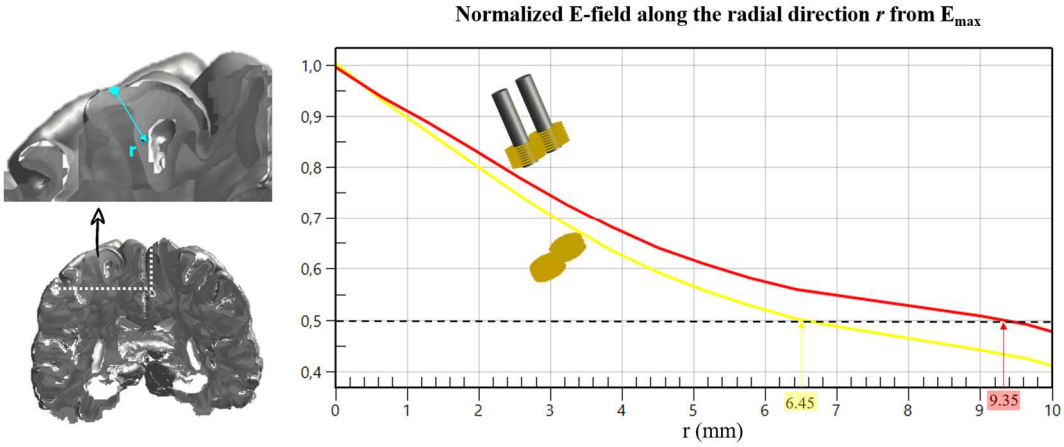

Figure 4. E-field trend along with the direction *r*, radial to the surface of the cortex from the peak point (right panel-cyan). Yellow curve: E-field induced by the *mCoil*. Red curve: E-field induced by the *mTMS* coil. The depth at which the normalized E-field value of 0.5 is crossed corresponds to the half value depth ($d_{1/2}$) defined in [24].

In **Fig. 4** we plotted the normalized E-field along the radial direction, originating at the target spot, and we showed that the crossing of $E_{max}/2$ occurs at 6.45 mm and 9.35 mm for the *mCoil* and the *mTMS* coil, respectively. Additionally, the two trends show that the *mTMS* coil (red curve) induced higher E-field intensities over the *mCoil* (yellow curve), with a difference that increases with the distance, confirming that E-field induced by the *mCoil* fades more rapidly. Finally, after estimating the penetration depth ($d_{1/2}$) as in **Fig. 4**, we calculated the focality as the half-value spread, $S_{1/2}$, as defined in [24] which resulted in 1.94 cm^2 for the mTMS and in 1.45 cm^2 for the *mCoil*.

4 Discussion and conclusions

We studied and compared two miniaturized figure-8 coils, the *mCoil*, and the *mTMS* coil. The first one elicited sensorial action potentials of healthy volunteers' radial nerve [20], [21]. The second one has been designed and manufactured to stimulate the central nervous system. To potentiate the *mCoil*, we doubled the number of copper traces, and we added an iron core. Consequently, the dimension of the miniaturized coil was increased by 1 cm. This work showed that the *mTMS* coil increases the penetration depth by 45% compared to the *mCoil* without affecting its focality that remained below 2 cm^2. The *mTMS* coils will allow us to both conduct animal studies more efficiently and to simultaneously and selectively stimulate several brain areas in humans, thanks to their reduced dimensions.

5 References

[1] A. Rotenberg, J. Horvath, and A. Pascual-Leone, *Transcranial Magnetic Stimulation Series Editor*. 2014.

[2] A. Valero-Cabré, J. L. Amengual, C. Stengel, A. Pascual-Leone, and O. A. Coubard, "Transcranial magnetic stimulation in basic and clinical neuroscience: A comprehensive review of fundamental principles and novel insights," *Neurosci. Biobehav. Rev.*, vol. 83, no. September, pp. 381–404, 2017.

[3] J. P. Lefaucheur *et al.*, "Evidence-based guidelines on the therapeutic use of repetitive transcranial magnetic stimulation (rTMS): An update (2014–2018)," *Clin. Neurophysiol.*, vol. 131, no. 2, pp. 474–528, 2020.

[4] R. Cavaleri, S. M. Schabrun, and L. S. Chipchase, "The number of stimuli required to reliably assess corticomotor excitability and primary motor cortical representations using transcranial magnetic stimulation (TMS): A systematic review and meta-analysis," *Syst. Rev.*, vol. 6, no. 1, pp. 1–11, 2017.

[5] M. E. Gunduz *et al.*, "Motor cortex reorganization in limb amputation: A systematic review of TMS motor mapping studies," *Front. Neurosci.*, vol. 14, no. April, 2020.

[6] J. Rösler *et al.*, "Language mapping in healthy volunteers and brain tumor patients with a novel navigated TMS system: Evidence of tumor-induced plasticity," *Clin. Neurophysiol.*, vol. 125, no. 3, pp. 526–536, 2014.

[7] K. Sakreida *et al.*, "High-resolution language mapping of Broca's region with transcranial magnetic stimulation," *Brain Struct. Funct.*, vol. 223, no. 3, pp. 1297–1312, 2018.

[8] M. Pitkänen, E. Kallioniemi, G. Järnefelt, J. Karhu, and P. Julkunen, "Efficient Mapping of the Motor Cortex with Navigated Biphasic Paired-Pulse Transcranial Magnetic Stimulation," *Brain Topogr.*, vol. 31, no. 6, pp. 963–971, 2018.

[9] T. Picht *et al.*, "Preoperative functional mapping for rolandic brain tumor surgery: Comparison of navigated transcranial magnetic stimulation to direct cortical stimulation," *Neurosurgery*, vol. 69, no. 3, pp. 581–588, 2011.

[10] K. Motomura *et al.*, "Navigated repetitive transcranial magnetic stimulation as preoperative assessment in patients with brain tumors," *Sci. Rep.*, vol. 10, no. 1, pp. 1–14, 2020.

[11] T. Wagner, J. Rushmore, U. Eden, and A. Valero-Cabre, "Biophysical foundations underlying TMS: Setting the stage for an effective use of neurostimulation in the cognitive neurosciences," *Cortex*, vol. 45, no. 9, pp. 1025–1034, 2009.

[12] K. Funke, "T009 Animal models of brain stimulation – TMS," in *Clinical Neurophysiology*, 2017, vol. 128, no. 3, pp. e3–e4.

[13] F. Cacace *et al.*, "Intermittent theta-burst stimulation rescues dopamine-dependent corticostriatal synaptic plasticity and motor behavior in experimental parkinsonism: Possible role of glial activity," *Mov. Disord.*, vol. 32, no. 7, pp. 1035–1046, 2017.

[14] J. Boonzaier, G. A. F. van Tilborg, S. F. W. Neggers, and R. M. Dijkhuizen, "Noninvasive Brain Stimulation to Enhance Functional Recovery After Stroke: Studies in Animal Models," *Neurorehabil. Neural Repair*, vol. 32, no. 11, pp. 927–940, 2018.

[15] A. Tang, G. Thickbroom, and J. Rodger, "Repetitive Transcranial Magnetic Stimulation of the Brain: Mechanisms from Animal and Experimental Models," *Neuroscientist*, vol. 23, no. 1, pp. 82–94, 2017.

[16] F. S. Salinas, J. L. Lancaster, and P. T. Fox, "3D modeling of the total electric field induced by transcranial magnetic stimulation using the boundary element method," *Phys. Med. Biol.*, vol. 54, no. 12, pp. 3631–3647, Jun. 2009.

[17] M. Talebinejad and S. Musallam, "Effects of TMS coil geometry on stimulation specificity," *2010 Annu. Int. Conf. IEEE Eng. Med. Biol. Soc. EMBC'10*, pp. 1507–1510, 2010.

[18] H. Tischler *et al.*, "Mini-coil for magnetic stimulation in the behaving primate," *J. Neurosci. Methods*, vol. 194, no. 2, pp. 242–251, 2011.

[19] L. M. Koponen and A. V Peterchev, "Transcranial Magnetic Stimulation: Principles and Applications," in *Neural Engineering*, B. He, Ed. Cham: Springer International Publishing, 2020, pp. 245–270.

[20] M. Colella *et al.*, "A microTMS system for peripheral nerve stimulation," in *Brain Stimulation*, 2019, vol. 12, no. 2, p. 521.

[21] M. Colella *et al.*, "Ultra-focal Magnetic Stimulation Using a μTMS coil: a Computational Study," *2019 41st Annu. Int. Conf. IEEE Eng. Med. Biol. Soc.*, pp. 3987–3990, 2019.

[22] M. Colella, M. Liberti, F. Apollonio, and G. Bonmassar, "A Miniaturized Ultra-Focal Magnetic Stimulator and Its Preliminary Application to the Peripheral Nervous System," in *Brain and Human Body Modeling 2020: Computational Human Models Presented at EMBC 2019 and the BRAIN Initiative® 2019 Meeting*, S. N. Makarov, G. M. Noetscher, and A. Nummenmaa, Eds. Cham: Springer International Publishing, 2021, pp. 167–176.

[23] M. I. Iacono *et al.*, "MIDA: A multimodal imaging-based detailed anatomical model of the human head and neck," *PLoS One*, 2015.

[24] Z. De Deng, S. H. Lisanby, and A. V. Peterchev, "Electric field depth-focality tradeoff in transcranial magnetic stimulation: Simulation comparison of 50 coil designs," *Brain Stimul.*, vol. 6, no. 1, pp. 1–13, 2013.